Semiconductor Electrodes

XIV. Electrochemistry and Electroluminescence at n-Type TiO_2 in Aqueous Solutions

Rommel N. Noufi,* Paul A. Kohl,* Steven N. Frank, and Allen J. Bard****

Department of Chemistry, The University of Texas, Austin, Texas 78712

ABSTRACT

The electrochemical behavior of single crystal n-TiO_2 was investigated in aqueous solutions. Charge transfer at the semiconductor/electrolyte interface was probed with several redox couples with standard redox potentials spanning a wide range. Most reductions occurred at potentials close to V_{fb}, the flatband potential and the current-voltage behavior suggested involvement of surface states in the charge transfer process. Evidence for the adsorption of phosphate ion and its effect on the reduction of $Fe(CN)_6^{3-}$ is also presented. Electroluminescence was observed during reduction of $S_2O_8^{2-}$ at wavelengths longer than 700 nm, suggesting the existence of intermediate levels.

The electrochemical behavior of n-TiO_2 has been the subject of several recent investigations including a previous report in this series (1), which utilized an aprotic solvent, acetonitrile (ACN), and which postulated that electron transfer can occur via intermediate levels or surface states within the bandgap region. Studies in aqueous solutions with TiO_2 (2) and other semiconductors (3, 4) have also investigated the mechanism of charge transfer of added redox couples at the semiconductor/solution interface. Although not as many Nernstian, one-electron redox couples are available in aqueous, as compared to nonaqueous solutions, the relative location of the energy levels of TiO_2 at the semiconductor/solution interface (*i.e.*, the flatband potential) can be changed in aqueous solutions by relatively large amounts by changing the solution *p*H. This provides another variable for investigating the band structure. This approach has previously been used to study SiC (4) and SnO_2 (5).

In the present study the semiconductor/solution interface was investigated by several techniques. Electron transfer reactions of couples, including some with standard redox potential well positive of those used in a previous study (2), were investigated at different *p*H's. To probe the existence and role of intermediate levels within the bandgap, electroluminescence of the n-TiO_2 semiconductor caused by electron-hole recombination from minority carrier injection from the electrolyte was studied. Hole injection into n-type semiconductors leading to radiative recombination has previously been demonstrated for GaP (6), SnO_2, ZnO, CdS, and GaAs (7).

In addition a study of the space charge capacitance, C_{sc}, as a function of potential, E, was undertaken in an attempt to determine the donor density (N_D) and flatband potential (V_{fb}), via the Schottky-Mott equation (Eq. [1]) (8)

$$1/C_{sc}^2 = (\Delta\phi_s - kT/e)\, 2/(\epsilon\epsilon_o e N_D) \qquad [1]$$

where C_{sc} is the space charge capacitance, $\Delta\phi_s$ is the amount of band bending, k is the Boltzmann constant, T is the absolute temperature, e is the electronic charge, ϵ is the dielectric constant of the semiconductor, and ϵ_o is the permittivity of free space. In several previous studies these plots of C_{sc}^{-2} *vs.* E showed deviations from the behavior predicted by Eq. [1] [see, for example, (2, 9, 10) and references therein]. In this work, two independent methods were used to calculate N_D for several n-TiO_2 crystals: (*i*) capacitance determined by a-c methods and cyclic voltammetry via Eq. [1] and (*ii*) conductance. Ohmic contacts were made by four different methods to determine their effect on the capacitance-potential behavior.

Experimental

The single crystal n-TiO_2 semiconductors used for the electrochemical investigation of redox couples were obtained from National Lead (Niagara Falls, New York). Two of the crystals were cut perpendicular to the C_2 axis and one of these was heated to 650°C in vacuum at 10^{-4} Torr for 3 hr and will be called "the moderately doped sample" with $N_D \simeq 10^{18}/cm^3$, as determined from a Schottky-Mott plot. The other was heated at 650°C in a hydrogen atmosphere for 15 min and will be denoted "the highly doped sample," with $N_D \cong 10^{20}/cm^3$. An ohmic contact was made to one side of each crystal by electrochemically depositing In from a 0.1M $InCl_3$ solution.

The capacitance measurements were made with four crystals cut perpendicular to the C_2 axis from a boule

* Electrochemical Society Student Member.
** Electrochemical Society Active Member.
Key words: semiconductors, luminescence, surface states.

generously donated by Fuji Titanium (Hiratsuka, Japan). The 1.5 mm thick crystals were heated in a hydrogen atmosphere for 15 min at 650°C. Two ohmic contacts were made to each crystal by one of the following methods:

1. Electrochemical deposition of indium from a 0.1M $InCl_3$ solution.
2. Electrochemical deposition of indium from a 0.1M $InCl_3$ solution followed by heating in vacuum (10^{-4} Torr) for 1 hr at 650°C.
3. Soldering a copper wire to the rear of the crystal with indium solder.
4. Smearing with In-Ga alloy (1:1 by volume mixture). In methods 1, 2, and 3, copper wires were attached to the contacts with conducting silver epoxy cement (Allied Corporation, New Haven, Connecticut).

The crystals were insulated, except for the (001) face, with Devcon epoxy cement (Devcon Corporation, Danvers, Massachusetts) and mounted on glass rods for use as electrodes as described previously (1). Each crystal was etched for about 15 sec in an HF/HNO_3 solution (11) prior to use except when special etchants were employed, as noted.

All compounds used in this study were reagent grade obtained from commercial sources. Solution concentrations were usually 1 and 10 m*M* in electroactive species. The solutions were prepared with triply distilled water and deaerated with prepurified nitrogen for 30 min. The electrochemical cell, similar to previous design (1), contained an optically flat Pyrex window for illuminating the semiconductor working electrode. A conventional three electrode design was used with an aqueous saturated calomel reference electrode (SCE) and a coiled platinum wire counterelectrode separated from the main compartment by a medium porosity glass frit. The capacitance measurements were performed in the dark with a platinum counterelectrode with an area at least ten times that of the working electrode. The d-c faradaic current was less than 0.2 $\mu A/cm^2$ in the voltage range used for capacitance measurements.

A PAR Model 173 potentiostat (Princeton Applied Research, Princeton, New Jersey) and PAR Model 175 universal programmer were used for the electrochemical measurements. Positive feedback was used to compensate for the *iR* drop in the solution and semiconductor working electrode. The cyclic voltammetric (*i-E*) curves were recorded on a Houston Instruments (Austin, Texas) Model 2000 X-Y recorder for scan rates less than 1 V/sec. For faster scan rates the *i-E* curves were recorded on a Tektronix Model 564 (Tektronix, Incorporated, Beaverton, Oregon) storage oscilloscope. The semiconductor electrodes were illuminated with a 450W xenon lamp (Oriel Corporation, Stamford, Connecticut) employing a Model 6242 power supply. The cell capacitance was measured by an a-c method which superimposed a 5 mV sine wave (500-10,000 Hz) on a d-c voltage, and corresponding phase shift between the current and voltage was measured with a PAR Model HR 8 lock-in amplifier. The potentiostat in these measurements was a Wenking Model 61 RH (G. Bank Elektronik, Germany), and the instrumental setup has been described previously (12). The capacitance was also estimated by measuring the charging current of the cyclic voltammograms in the absence of electroactive species as discussed in the next section.

The electroluminescence emitted in the ultraviolet and visible region was detected with a Barr and Stroud (Glasgow, United Kingdom) circular interference filter and a sensitive photomultiplier tube (Dumont 6467). The near infrared light was detected with an Oriel Model 7240 grating monochromator (grating blazed at 1 μm) in conjunction with an ultraviolet cut off filter and Radiometer/photometer (E. G. & G. Incorporated, Salem, Massachusetts).

Results

Capacitance measurements.—The d-c and a-c current measured between the two contacts made on the crystals was directly proportional to the applied voltage and independent of polarity and frequency over the range 100-10,000 Hz for all of the contacts. Thus these can be taken as purely ohmic contacts.

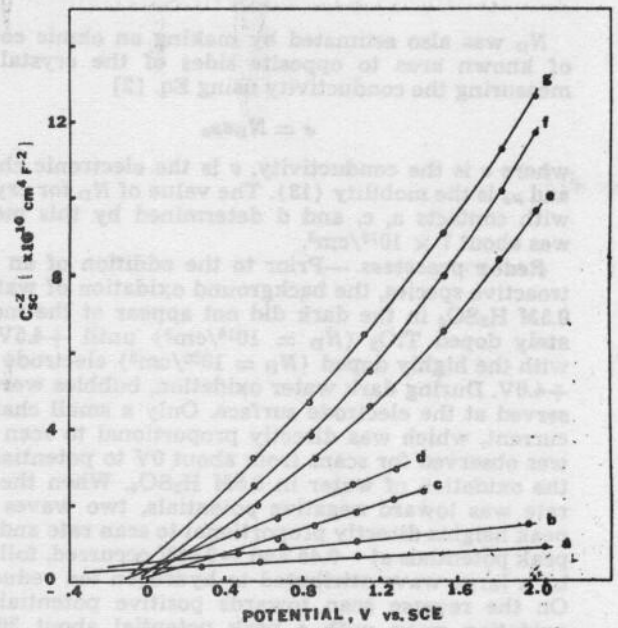

Fig. 1. Plot of C_{sc}^{-2} (cm^4F^{-2}) *vs.* *E* (V, *vs.* SCE) in 1.0M H_2SO_4. Capacitance measured by (a) a-c method at 500 Hz, (b) a-c method at 1000 Hz, (c) cyclic voltammetric method at 5 V/sec, (reactivated crystal), (d) cyclic voltammetric method at 500 V/sec (reactivated crystal), (e) a-c method 1000 Hz (reactivated crystal), (f) a-c method 2000 Hz (reactivated crystal), (g) a-c method 5000 Hz (reactivated crystal).

Plots of C_{sc}^{-2} *vs.* *E* (Eq. [1]) of a moderately doped TiO_2 crystal under various conditions are shown in Fig. 1. Curves a and b were obtained by a-c methods at 500 and 1000 Hz, respectively, after the crystal had been used for extended periods as a photoanode in a 1.0M H_2SO_4 solution. The current density of these photoanodes decreased with time during irradiation, as previously reported (10). When the crystal was reactivated in vacuum (10^{-4} Torr) at 650°C for 5 min, the C_{sc}^{-2} *vs.* *E* plots shown in Fig. 1, curves e, f, and g resulted. C_{sc} was also estimated from the charging current measured in the cyclic voltammograms in the dark at various scan rates (0.2-500 V/sec) with no electroactive species in solution. The capacitance was calculated by dividing the current at a given potential by the scan rate. Curves c and d (Fig. 1) show the C_{sc}^{-2} *vs.* *E* plots at 5 and 500 V/sec respectively, for a reactivated crystal.

The Schottky-Mott plots for the four crystals with the different types of contacts (see experimental section) were all very similar with the exception of contact b which yielded a smaller slope, apparently because the doping level increased during the heating in vacuum. The donor densities calculated from the a-c measurements (500-10,000 Hz) for contacts a, c, and d were $1 \times 10^{20}/cm^3$ to $2 \times 10^{20}/cm^3$, while the cyclic voltammetry results (0.2-500 V/sec) gave values of $2 \times 10^{20}/cm^2$ to $3 \times 10^{20}/cm^3$. In all cases, frequency dispersion of the C_{sc}^{-2} *vs.* *E* plots was observed with both the a-c and cyclic voltammetric results.

The intersection of the C_{sc}^{-2} *vs.* *E* plot with the x-axis, yielding V_{fb}, was very similar for the a-c methods and cyclic voltammetric results but there was appreciable scatter and frequency dependence in the V_{fb} values obtained by extrapolation. The origin of the frequency dispersion has been studied extensively and several reasons have been given for the observed results, *e.g.*, dielectric relaxation, crystal imperfections, adsorbed species, and filling and emptying of localized levels in the bandgap (2, 9, 10).

N_D was also estimated by making an ohmic contact of known area to opposite sides of the crystal and measuring the conductivity using Eq. [2]

$$\sigma = N_D e \mu_e \quad [2]$$

where σ is the conductivity, e is the electronic charge, and μ_e is the mobility (13). The value of N_D for crystals with contacts a, c, and d determined by this method was about $7 \times 10^{19}/cm^3$.

Redox processes.—Prior to the addition of an electroactive species, the background oxidation of water in 0.5*M* H_2SO_4 in the dark did not appear at the moderately doped TiO_2 ($N_D = 10^{18}/cm^3$) until +4.5V and with the highly doped ($N_D = 10^{20}/cm^3$) electrode until +4.0V. During dark water oxidation, bubbles were observed at the electrode surface. Only a small charging current, which was directly proportional to scan rate, was observed for scans from about 0V to potentials for the oxidation of water in 0.5*M* H_2SO_4. When the scan rate was toward negative potentials, two waves with peak heights directly proportional to scan rate and with peak potentials at −0.45 and −0.85V occurred, followed by a large wave attributed to hydrogen ion reduction. On the reverse scan towards positive potentials, an oxidation wave with a peak potential about 30 mV positive of the first reduction peak appeared; this was attributed to the oxidation of hydrogen. These reduction and oxidation peaks shifted towards negative potentials by about 30 mV/pH unit with increasing pH.

The charge transfer processes at the n-TiO_2/electrolyte interface were studied using several redox systems, listed in Table I. Representative examples of cyclic voltammograms for reductions are shown in Fig. 2. The reduction of $Fe(CN)_6^{3-}$, Ce^{4+}, Fe^{3+}, Ag^{2+}, and $IrCl_6^{2-}$ did not start until the electrode potential was well negative of the corresponding $E_{1/2}$ value ($E_{1/2}$ is taken here as $(E_{pc} + E_{pa})/2$) determined at Pt. In all cases the wave was shifted towards V_{fb} which was not changed by the addition of any of the redox systems, but some current flow occurred at potentials positive of V_{fb}. No reversal anodic waves were found for any reduction. For all waves the reduction peak currents varied with the square root of the scan rate, $v^{1/2}$, and the cathodic peak potentials (E_{pc}) shifted negative by about 54 mV/pH unit. The E_{pc} values for the moderately doped TiO_2 electrode were always 20-70 mV more negative of those for the highly doped one at the same pH. The cathodic current density depended exponentially on the applied potential in a region at the foot of the wave near, but positive of V_{fb}. From Tafel plots, *i.e.*, log i_c *vs.* E, as shown in Fig. 3, which were obtained from the exponential current rise in a stirred solution where there was no contribution from mass transfer, the transfer coefficient, α, was calculated, assuming Eq. [3] applies

Table I. Peak potentials (vs. SCE) for the reduction and reoxidation of compounds used in this study. The scan rate was 0.1 V/sec the donor density of the n-TiO_2 was $N_D = 10^{18}/cm^3$

Compound	Electrolyte	Pt E_{pc}	Pt E_{pa}	n-TiO_2 E_{pc}
$IrCl_6^{2-}$	6*M* HCl	0.98	1.36	0.02
Ag^{2+}	4*M* HNO_3	1.06	1.21	−0.02
Ce^{4+}	0.5*M* H_2SO_4	0.70	—	−0.12
$Fe(CN)_6^{3-}$	0.5*M* H_2SO_4	0.40	0.52	−0.24
Fe^{3+}	0.5*M* H_2SO_4	0.36	0.48	−0.31

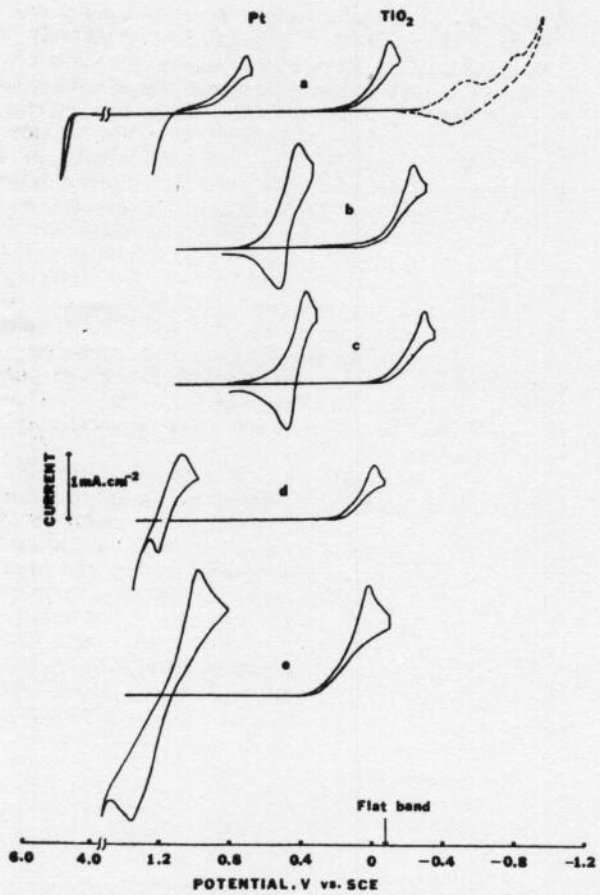

Fig. 2. Cyclic voltammograms for moderately doped ($N_D = 10^{18}/cm^3$) TiO_2 and Pt disk electrodes in (– – – –) 0.5M H_2SO_4 and (————) 0.5M H_2SO_4 with (a) 10^{-2}M Ce^{4+}, (b) 10^{-2}M $Fe(CN)_6^{3-}$, (c) 10^{-2}M Fe^{3+}, (d) 10^{-2}M Ag^{2+}, (e) 10^{-2}M $IrCl_6^{2-}$ at a sweep rate of 0.1 V/sec.

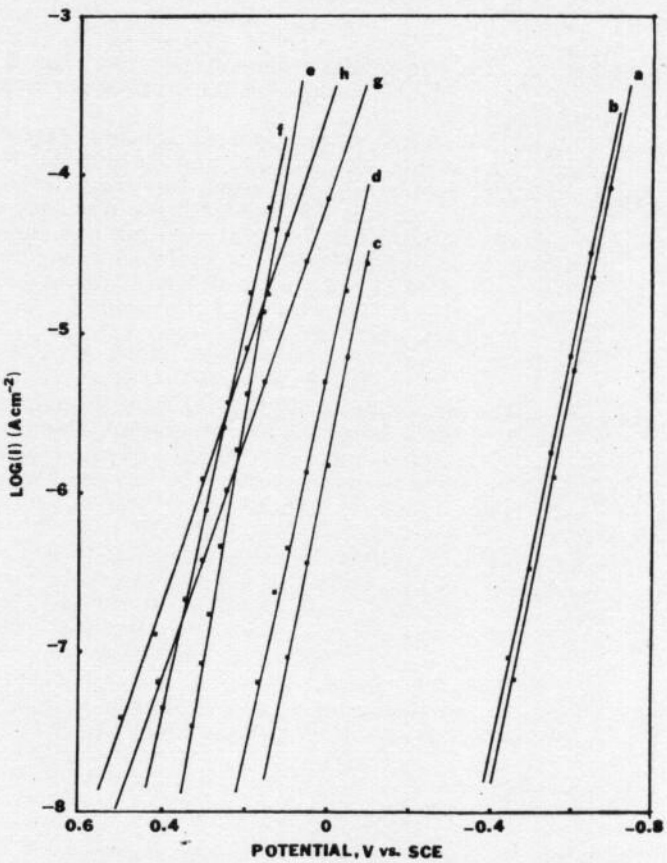

Fig. 3. Logarithm of the dark cathodic current *vs.* applied potential for the highly doped (H.D.) ($N_D = 10^{20}/cm^3$) and moderately doped (M.D.) ($N_D = 10^{18}/cm^3$) n-TiO_2 electrodes. (a) 10^{-2}M $Fe(CN)_6^{3-}$, 0.1M KOH, M.D. (b) 10^{-2}M $Fe(CN)_6^{3-}$, 0.1M KOH, H.D. (c) 10^{-2}M $Fe(CN)_6^{3-}$, 0.5M H_2SO_4, M.D. (d) 10^{-2}M $Fe(CN)_6^{3-}$, 0.5M H_2SO_4, H.D. (e) 10^{-1}M Ag^{2+}, 4M HNO_3, M.D. (f) 10^{-1}M Ag^{2+}, 4M NHO_3, H.D. (g) 10^{-2}M Ce^{4+}, 0.5M H_2SO_4, M.D. (h) 10^{-2}M Ce^{4+}, 0.5M H_2SO_4, H.D.

Table II. Comparison of the dark cathodic behavior of oxidizing agents at highly doped (H.D.) and moderately doped (M.D.) n-TiO_2 single crystals[a]

Oxidizing agent	Conc	$E_{1/2}$[b] on Pt (-V vs. SCE)	Electrolyte	α H.D.	α M.D.	i° (A cm^{-2}) H.D.	i° (A cm^{-2}) M.D.
Ag^{2+}	0.1*M*	1.14	4*M* HNO_3	0.75	0.85	$<10^{-15}$	
$IrCl_6^{2-}$	0.01*M*	1.17	6*M* HCl	0.35	0.35	4×10^{-10}	6×10^{-11}
Ce^{4+}	0.01*M*	0.82[c]	0.5*M* H_2SO_4	0.42	0.42	2×10^{-10}	1×10^{-11}
$Fe(CN)_6^{3-}$	0.01*M*	0.46	0.5*M* H_2SO_4	0.75	0.80	8×10^{-10}	7×10^{-11}
Fe^{3+}	0.01*M*	0.42	0.5*M* H_2SO_4	0.44	0.46	2×10^{-7}	4×10^{-9}

[a] H.D., highly doped ($N_D \sim 10^{20}$ cm^{-3}); M.D., moderately doped ($N_D \sim 10^{18}$ cm^{-3}).
[b] $E_{1/2}$ is taken here as $(E_{pc} + E_{pa})/2$.
[c] Half-peak potential.

$$\log i_c = \log i^\circ - \frac{\alpha n F (E - E_{1/2})}{2.3\,RT} \qquad [3]$$

where n is the number of equivalents per mole, F is Faraday's constant, R is the ideal gas constant, and T is the absolute temperature. The exchange current, i°, was estimated by extrapolation of log i_c to the $E_{1/2}$ value found with a platinum electrode for the redox couple. A summary of the Tafel plot results is given in Table II. The values of the Tafel slope, $(dE/d \log i)$, for the different couples were relatively high for TiO_2 compared to values found with other semiconductors as was also observed by Gomes *et al.* (2). The accepted model (8), which assumes isoenergetic electron transfer of an electron from the semiconductor conduction band to unoccupied solution levels predicts a slope of 60 mV ($\alpha = 1$) for a pure conduction band process at potentials positive of V_{fb}.

Effect of supporting electrolyte.—The cyclic voltammetric reduction of $Fe(CN)_6^{3-}$ in buffers containing phosphate in the pH range 5-9.5 showed two peaks at TiO_2 (Fig. 4a), but only one at Pt in this buffer. The relative height of the two peaks was a function of scan rate (Fig. 4b) and also of the etchant employed. The more positive peak (P_1) was higher at lower scan rates and also when the electrode was etched in 5*M* NaOH as compared to a concentrated HNO_3 etchant. The second peak was more pronounced after etching in concentrated HNO_3 and at higher scan rates. Addition of Na_2SO_4 or KI to the phosphate electrolyte suppressed the second wave (P_2) until only the first wave appeared during reduction. Only the first wave was observed with other electrolytes (*e.g.*, 0.5*M* H_2SO_4, 0.1*M* KOH). Addition of Na_2SO_4 to produce a solution concentration of 0.2*M* totally suppressed the second wave in 0.33*M* phosphate buffer with an electrode etched in HNO_3. The addition of KCl to the buffer however did not have any effect on the double wave. Other redox couples such as $CuCl_2$, Ce^{4+}, and $IrCl_6^{2-}$ did not exhibit the double wave phenomenon in the phosphate buffers. However, experiments with these required acidic media, and at these pH's even $Fe(CN)_6^{3-}$ did not show the double wave. $Fe(C_2O_4)_3^{3-}$ and Fe^{3+} also exhibited a similar double wave behavior. However, for these the two waves were not as well defined as those found with $Fe(CN)_6^{3-}$; in this case the first wave was shifted towards negative potentials, so that it appeared as a prewave on the second wave and quantitative data on the relative peak heights was not possible. A systematic change of the total phosphate concentration from 0.01 to 0.5*M* at a fixed *pH* did not appear to change V_{fb}, as determined by the onset of photoanodic current.

Oxidation.—When the electrode was scanned to potentials positive of V_{fb}, a blocking region was observed in the dark extending to +4.5 and +4.0V *vs.* SCE for the moderately and highly doped electrodes respectively, where no oxidation currents appeared. In Fig. 5 the effect of addition of the reduced forms of several redox couples on the dark anodic current is shown and the behavior of the highly doped electrode is compared to that of the moderately doped one. At the highly doped electrode the blocking region was smaller than that of the moderately doped one with no reducing agent in solution. Upon addition of a reducing agent, an anodic current started at less positive potentials than background oxidation for all species tried at the highly doped electrode. At the moderately doped electrode only $Fe(CN)_6^{4-}$ produced significant anodic current at potentials less positive than the background oxidation; the oxidations of Ce^{3+} and Fe^{2+}, if they occurred, took place along with the background oxidation.

Illumination of the electrode did not have any effect on the reduction processes. Oxidation of the reduced species occurred upon illumination which was evident by the increase in the anodic current at a given potential on the rising portion of the wave for photooxidation of water, which commences positive of V_{fb}. A decrease in the amount of O_2 evolved was observed, indicating competition of the reduced species with water for the photogenerated holes. These types of

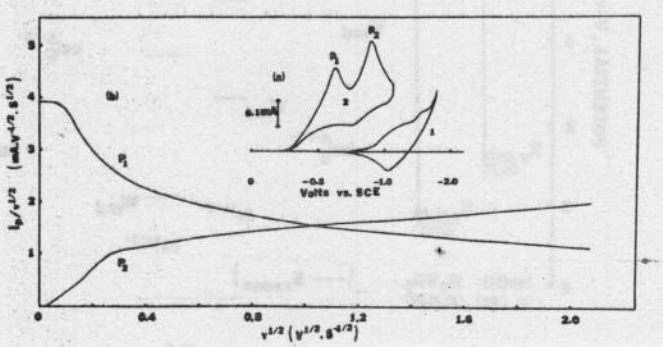

Fig. 4. (a) Cyclic voltammogram at 0.1 V/sec of n-TiO_2 ($N_D = 10^{18}$/cm^3) (etched in concentrated HNO_3), 0.33*M* phosphate buffer, *pH* = 7.3. (1) alone and (2) containing 10 mM $Fe(CN)_6^{3-}$; (b) peak current dependence *vs.* scan rate, conditions as (a) (2).

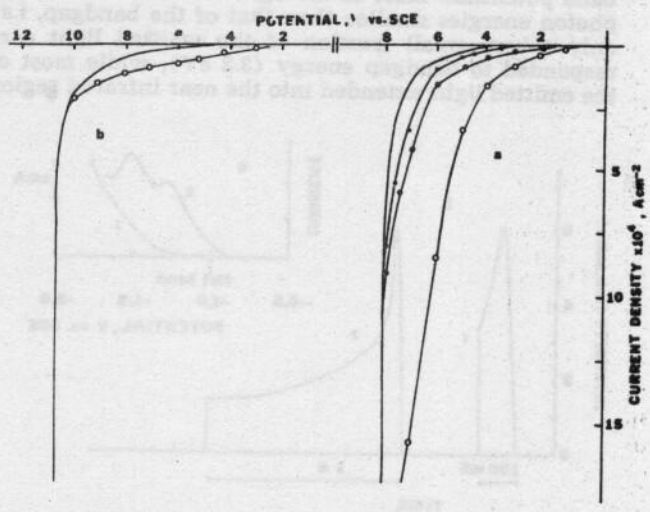

Fig. 5. Linear potential sweep in (———) 0.5*M* H_2SO_4 containing (○) 0.2*M* $Fe(CN)_6^{3-}$, (●) 0.2*M* Fe^{2+}, (■) 0.2*M* Ce^{3+} at TiO_2. (a) Highly doped ($N_D = 10^{20}$/cm^3), (b) moderately doped ($N_D = 10^{18}$/cm^3).

experiments on photoprocesses for different redox couples in aqueous solutions at TiO_2 have been discussed elsewhere (14, 15).

Polycrystalline TiO_2 prepared by chemical vapor deposition (16) showed identical electrochemical behavior in aqueous solution to that of the moderately doped single crystal. Similar results have already been demonstrated in acetonitrile (1). However, the photocurrents on the polycrystalline electrodes were smaller than those for the single crystals.

Light emission.—The electroluminescence observed during reduction of persulfate and H_2O_2 at several semiconductors in aqueous solutions has been used to interpret the mechanism of charge transfer and to obtain information about energy levels in the gap (6, 7). Luminescence produced by recombination of an electron with a hole in the semiconductor was also observed with n-TiO_2 electrodes when persulfate was reduced. The mechanism for luminescence probably follows that proposed for other semiconductors (6, 7) with an initial step being transfer of an electron from the conduction band or a surface state below the conduction band to $S_2O_8^{2-}$ (Eq. [4])

$$S_2O_8^{2-} + e^-(CB) \rightarrow SO_4^{2-} + SO_4^{\cdot -} \qquad [4]$$

Since $SO_4^{\cdot -}$ is very easily reduced, the $SO_4^{\cdot -}/SO_4^{2-}$ energy level lies below the valence bandedge, and thus electron transfer to the radical causes injection of a hole into the valence band or a state just above the valence band (Eq. [5])

$$SO_4^{\cdot -} \rightarrow SO_4^{2-} + h^+(VB) \qquad [5]$$

Electron-hole recombinations then cause emission of radiation. The *i-E* curve (Fig. 6a) shows that the reduction of persulfate occurs about 100 mV positive of the background reduction of water. The light emission did not start when the reduction of persulfate first occurred. Luminescence began when the electrode potential was pulsed to −1.5V, a value negative of V_{fb}. The emission intensity increased with pulsing to more negative potentials and attained a maximum value at −3.0V. At this potential the intensity was a function of pulse duration and was largest with a 100 msec pulse. Shorter pulses gave weak emission; longer pulses gave an emission with intensity equal to that of the 100 msec pulse which then decayed to a steady state (Fig. 6b). The TiO_2 electroluminescence spectra (Fig. 7) were different than those observed with ZnO (7), although both materials have similar bandgaps and flatband potentials. Most of the light emission occurred at photon energies smaller than that of the bandgap, *i.e.*, only a very small fraction of the emitted light corresponded to bandgap energy (3.2 eV), while most of the emitted light extended into the near infrared region

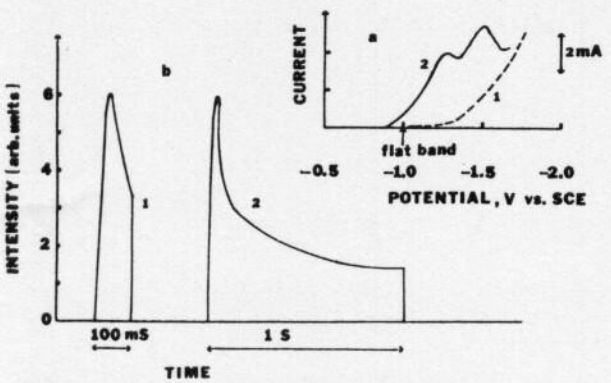

Fig. 6. (a) Linear potential sweep of highly doped n-TiO_2 at 0.1 V/sec in (1) 5M NaOH solution, (2) 0.1M $S_2O_8^{2-}$, 5M NaOH solution, (b) Intensity *vs.* time curve of the electroluminescence of n-TiO_2 at −3.0V in 0.1M $Na_2S_2O_8$, 5M NaOH (1) 0.1 sec pulse, (2) 1 sec pulse.

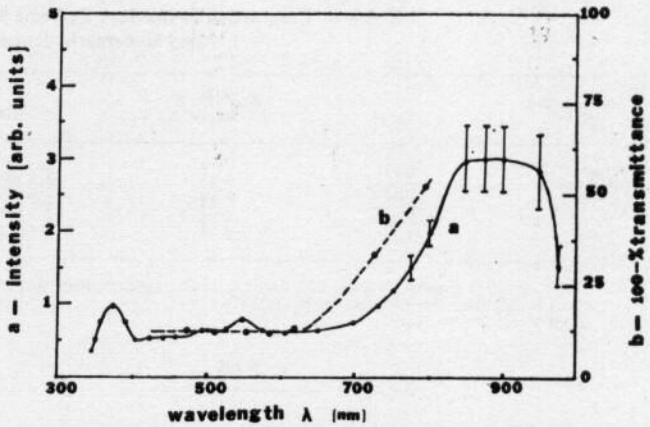

Fig. 7. (a) Spectral distribution of electroluminescence of n-TiO_2 at −3.0V with grating monochromator, (b) percent transmission of electroluminescence at −3.0V with cut-on filters.

with photon energies of 1.5-1.24 eV. This behavior is similar to that exhibited by n-GaAs (7).

The spectral distribution of the luminescence with n-TiO_2 clearly suggests the existence of surface states or intermediate levels located within the bandgap. As in the previous studies (6, 7), the quantum efficiency for the emission is very low suggesting that the extent of nonradiative recombination or reduction of $SO_4^{\cdot -}$ directly via surface states rather than via the valence band is significant. Previous studies of TiO_2 (1, 14) and other semiconductors (17) in nonaqueous solvents have provided evidence of the importance of levels within the gap in explaining the electrochemical properties of semiconductor materials.

Discussion

Reduction.—The reduction of solution species in the absence of surface states should occur at a wide bandgap semiconductor through either the conduction band or valence band depending upon the standard potential of the redox couple (8). The position of the energy levels and distribution maxima of the solution species investigated and TiO_2 are shown in Fig. 8, where W_{Ox} is the maximum of the distribution for the oxidized form in solution, W_{Red} is the maximum of the distribution for the reduced form, and $E°_{redox}$ is the Fermi level of the redox couple (8). The separation between

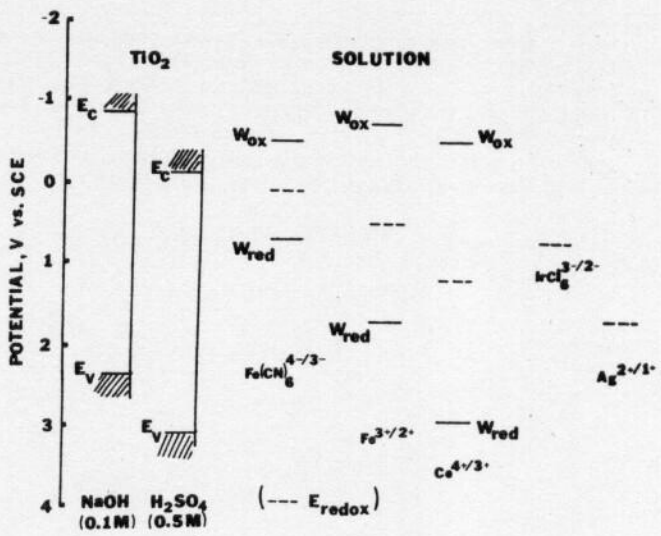

Fig. 8. Relative energy positions of n-TiO_2 and various redox couples where $E°_{redox}$ is the standard redox potential, W_{Red} is the distribution maximum of the reduced species, W_{Ox} is the distribution maximum of the oxidized species, E_c and E_v are the conduction and valence bandedges, respectively.

W_{Ox} and W_{Red} is essential 2λ, where λ is the solvent reorganizational energy during electron transfer. The λ values estimated for several couples by Memming *et al.* (5) have been used in Fig. 8. For all of the couples in this study the distribution of the oxidized form at the valence bandedge, $W_{Ox}(E_v)$, is small so that reduction by hole injection into the valence band should be small. However, for reduction only via the conduction band for a couple where E°_{redox} is below E_c the reduction current should be proportional to the electron density at the surface, n_s, and the overlap of the unoccupied solution levels with the conduction band, $W_{Ox}(E_c)$. The potential dependence of the reduction current should then follow that of n_s and hence the apparent exchange parameter, α (as defined in Eq. [3]) should be equal to unity at potentials positive of V_{fb}. Since α values less than one were observed, a pure conduction band process seems unlikely. We do not think that reduction via tunneling from the conduction band to the oxidized species, as discussed by Pettinger *et al.* (18) is likely in this case. Our results show that the reduction current for $Fe(CN)_6^{3-}$ in both 0.5*M* H_2SO_4 and 0.1*M* KOH starts positive of V_{fb} by about 0.45V. Tunneling from the conduction band to solution, which is a function of the space charge thickness at the energy level distribution of the unoccupied species (18), should give a larger difference between the onset of the reduction current and V_{fb} (because of the negative shift in V_{fb}) in base as compared to acid while the distribution W_{Ox} remains fixed. The onset of reduction on both the highly and moderately doped TiO_2 crystals occurs at potentials where the extent of band bending appears to be too small to satisfy the conditions for such tunneling. Thus the α values measured probably represent involvement of surface states or intermediate levels in the reduction processes. Dutoit *et al.* (2) also found anomalously large Tafel slopes for the reduction of several couples at n-TiO_2 and presented strong arguments against variation of the Helmholtz layer potential as the origin of this effect.

The reduction of electroactive species with redox potentials well positive of V_{fb} at both moderately and highly doped TiO_2, in aqueous solutions is different from the behavior found in ACN (1). In ACN couples with redox potentials more than 1.5V positive of V_{fb} were all reduced at potentials about 1V below the conduction bandedge; this was attributed to the location of intermediate levels in the semiconductor near this energy. The redox couples used in this study with $|E_{redox} - V_{fb}|$ greater than 1.2V all showed reduction waves close to V_{fb} (Fig. 2). However, the solvent interaction energy, λ, is larger in water than in ACN. This broadens the W_{Ox} distribution and shifts it closer to the conduction band, making better overlap possible even for couples with very positive values of E_{redox} (Fig. 8). Couples with potentials as positive as those used in ACN could not be employed because they are not stable in water. It is also possible that the different extent of interaction of the water with the TiO_2 surface causes the energy level of surface states to be located closer to the conduction band than in ACN.

The double wave for the reduction of $Fe(CN)_6^{3-}$ in the phosphate-containing media can be attributed to the adsorption of phosphate on the TiO_2 surface and reduction of $Fe(CN)_6^{3-}$ at both phosphate-free and phosphate-covered sites. At the free sites the reduction occurs at similar potentials as found in other supporting electrolytes while at the covered sites the reduction takes place at more negative potentials. The double wave cannot be attributed to solution chemistry, since the behavior at the platinum electrode is the same as in other media, and no type of interaction between $Fe(CN)_6^{3-}$ and a phosphate is apparent. The effect of etchant noted on the double-wave behavior can probably be explained by changes in the extent of adsorption of phosphate with surface treatment with the acidic etchant (concentrated HNO_3) enhancing the adsorption of phosphate as compared to the basic one (5*M* NaOH). The scan rate dependence of the two peaks can be explained qualitatively by considering the two site reduction as analogous to a reversible preceding chemical reaction (CE). P_1 represents the reduction of $Fe(CN)_6^{3-}$ on free sites and P_2 represents the reduction on phosphate-covered ones. At slow scan rates reduction occurs mainly via the free sites, since $Fe(CN)_6^{3-}$ has time to diffuse to these locations; thus $P_1 > P_2$. At fast scan rates reduction occurs via both sites and the ratio of P_2 to P_1 increases (Fig. 4). Note, however, that the total peak height ($P_1 + P_2$) is constant, proportional to the total electrode area at all scan rates.

Oxidations.—The oxidation of a number of couples in the dark at TiO_2 and other wide bandgap semiconductors (2, 18-20) has been explained by tunneling from filled levels in the electrolyte to empty levels at the same energy in the conduction band. Our results are in agreement with this explanation. The tunneling of electrons from solution species does not occur until the thickness of the space charge region, X, (which is a function of the surface field strength and N_D as shown in Eq. [6]) at the energy level of the reduced species becomes sufficiently thin (18, 21). The steep increase in the anodic current for water oxidation beyond a band bending equivalent to the bandgap of TiO_2 (3.2 eV) is a result of interband tunneling (22)

$$X = (2\epsilon_o\epsilon\Delta\phi/eN_D)^{1/2} \quad [6]$$

The anodic current in the blocking region upon the addition of a reducing agent increases as a result of a tunneling process at an energy where the distribution for reduced form in solution is sufficiently large and the extent of band bending is such that the space charge thickness is sufficiently small. The observed results agree very well with previous studies and with the relative energy positions of the occupied levels (Fig. 8) below the conduction band.

Acknowledgment

The support of this research by the National Science Foundation and the Army Research Office is gratefully acknowledged.

Manuscript submitted July 15, 1977; revised manuscript received Sept. 2, 1977.

Any discussion of this paper will appear in a Discussion Section to be published in the December 1978 JOURNAL. All discussions for the December 1978 Discussion Section should be submitted by Aug. 1, 1978.

Publication costs of this article were assisted by the National Science Foundation and Army Research Office.

REFERENCES

1. S. N. Frank and A. J. Bard, *J. Am. Chem. Soc.*, **97**, 7427 (1975).
2. E. C. Dutoit, F. Cardon, and W. P. Gomes, *Ber. Bunsenges. Phys. Chem.*, **80**, 475 (1976).
3. W. P. Gomes and F. Cardon, *Z. Phys. Chem.*, **86**, 330 (1973).
4. M. Gleria and R. Memming, *J. Electroanal. Chem.*, **65**, 163 (1975).
5. R. Memming and F. Mollers, *Ber. Bunsenges. Phys. Chem.*, **76**, 475 (1972).
6. K. H. Beckman and R. Memming, *This Journal*, **116**, 368 (1969).
7. B. Pettinger, H. R. Schoppel, and H. Gerischer, *Ber. Bunsenges. Phys. Chem.*, **80**, 849 (1976).
8. (a) H. Gerischer, in "Physical Chemistry: An Advance Treatise," Vol. 9A, H. Eyring, D. Henderson, and W. Jost, Editors, Academic Press, New York (1970); (b) H. Gerischer, *Adv. Electrochem. Electrochem. Eng.*, **1**, 139 (1961).
9. E. C. Dutoit, R. L. Van Meirhaege, F. Cardon, and W. P. Gomes, *Ber. Bunsenges. Phys. Chem.*, **79**, 1206 (1976).
10. L. A. Harris and R. H. Wilson, *This Journal*, **123**, 1010 (1976).
11. A. Fujishima, K. Honda, and S. Kikuchi, *Chem. Soc. Jpn.*, **72**, 108 (1969).
12. H. Kojima and A. J. Bard, *J. Electroanal. Chem.*, **63**, 117 (1975).

13. R. G. Breckenridge and W. R. Hosler, *Phys. Rev.*, **91**, 793 (1953).
14. S. N. Frank and A. J. Bard, *J. Am. Chem. Soc.*, **99**, 4669 (1977).
15. E. C. Dutoit, F. Cardon, and W. P. Gomes, *Ber. Bunsenges. Phys. Chem.*, **80**, 1285 (1976).
16. K. L. Hardee and A. J. Bard, *This Journal*, **122**, 739 (1975).
17. P. A. Kohl and A. J. Bard. *J. Am. Chem. Soc.*, **99**, 7531 (1977).
18. B. Pettinger, H. R. Schoppel, and H. Gerischer, *Ber. Bunsenges. Phys. Chem.*, **78**, 450 (1974).
19. P. J. Boddy, *This Journal*, **115**, 199 (1968).
20. F. Mollers and R. Memming, *Ber. Bunsenges. Phys. Chem.*, **76**, 469 (1972).
21. J. F. Dewald, *J. Phys. Chem. Solids*, **14**, 155 (1960).
22. B. Pettinger, H. R. Schoppel, T. Yokoyama, and H. Gerischer, *Ber. Bunsenges. Phys. Chem.*, **78**, 1024 (1974).